Optics Letters

Phase-shifted fiber Bragg grating modulated by a hollow cavity for measuring gas pressure

Junxian Luo,[1,2] Shen Liu,[1,2,3,*] Yuanyuan Zhao,[1,2] Yanping Chen,[1,2] Kaiming Yang,[1,2] Kuikui Guo,[1,2] Jun He,[1,2,3] Changrui Liao,[1,2,3] and Yiping Wang[1,2,3]

[1]Guangdong and Hong Kong Joint Research Centre for Optical Fibre Sensors, College of Physics and Optoelectronic Engineering, Shenzhen University, Shenzhen 518060, China
[2]Guangdong Laboratory of Artificial Intelligence and Digital Economy (SZ), Shenzhen University, Shenzhen 518060, China
[3]Key Laboratory of Optoelectronic Devices and Systems of Ministry of Education and Guangdong Province, Shenzhen University, Shenzhen 518060, China
*Corresponding author: shenliu@szu.edu.cn

Received 28 October 2019; revised 25 November 2019; accepted 1 December 2019; posted 5 December 2019 (Doc. ID 381452); published 10 January 2020

A gas pressure sensor, based on a phase-shifted fiber Bragg grating (PS-FBG) modulated by a hollow cavity, is proposed and demonstrated in this Letter. The device was fabricated by fusing a hollow-core fiber (HCF) between two single-mode fibers (SMFs) exhibiting FBGs that were inscribed using line-by-line femtosecond (fs) laser etching. A pair of micro-channels were drilled orthogonally into the HCF using an fs laser to allow the argon gas to get in and out freely. Such a sensor exposes a high spectrum finesse, e.g., a *Q*-factor of ∼7302, which can be improved by increasing the grating pitch quantity. Furthermore, a high gas pressure sensitivity of 1.22 nm/Mpa is obtained, corresponding the improved sensor with a grating pitch quantity of 300 and a hollow cavity length of 88.3 μm. In addition, the device exhibited a low temperature sensitivity of 8.92 pm/°C.

https://doi.org/10.1364/OL.381452

Gas pressure is an essential physical parameter in a variety of industrial applications. In recent years, various types of gas pressure sensors have been reported, such as those based on bare fiber Bragg gratings (FBGs) [1,2], hollow-core photonic bandgap fibers [3], optical fiber Fabry–Perot interferometers (FPIs) [3–5], hollow eccentric twin-core optical fibers [6], a fiber tip air bubbles [7,8], and ultra-thin sensing films [9–11]. However, these devices have inherent disadvantages and limitations. For example, FPI sensors exhibit low spectral fineness due to low reflectivity (∼3.5%) of the optical fiber end. In many applications, the full width at half maximum (FWHM) of the spectral lines is of special interest when evaluating system performance, which is related to both the cavity finesse and quality factor (*Q*-factor). Techniques for improving these metrics have been reported recently, including a study by Malak *et al.*, which demonstrated enhanced reflectance by installing two groups of cylindrical Bragg mirrors to form a multilayer resonator [12]. Jiang *et al.* reported a multi-beam interferometric FPI based on TiO2 nanoparticle-coated thin films [13]. FBGs are among the most successful optical fiber devices, attracting significant attention due to their high *Q*-factors. Interestingly, phase-shifted FBGs (PS-FBGs) exhibit a narrower FWHM than FBGs. As such, a variety of optical components based on PS-FBGs have been developed for applications to multi-channel notch filters [14], distributed feedback FBG Raman lasers [15], radio frequency (RF) signal detection [16], continuous detection of micro-particles [17], and ultrasonic imaging [18]. Nevertheless, optical gas pressure sensors based on PS-FBGs have not been reported, and it would be of great potential if the PS-FBG with high spectral fineness be used in optical fiber-sensing field.

This study proposes and experimentally demonstrates, to the best of our knowledge, a novel gas pressure sensor that is based on a PS-FBG modulated by an in-fiber hollow cavity. The resulting device sensitivity and *Q*-factor were improved significantly by balancing the length of the hollow cavity and the FBG pitch quantity. The resulting *Q*-factor improved to ∼7302, making the proposed sensor more suitable for dynamic monitoring of gas pressure than conventional designs. A gas pressure sensitivity of 1.22 nm/Mpa was also achieved with a grating pitch quantity of 300 and a hollow cavity length of 88.3 μm. In addition, the device exhibited a temperature sensitivity of 8.92 pm/°C.

Figure 1(a) illustrates the structure of the proposed gas pressure sensor based on a PS-FBG, modulated by a hollow cavity. The device fabrication process involved three steps. In the first step, an in-fiber hollow cavity was produced by splicing a hollow-core fiber (HCF) with two standard single-mode fibers (SMFs) using a commercial fusion splicer. The HCF had an inner diameter of 75 μm, an outer diameter of 125 μm, and well-cleaved ends. This step produced a gas cavity in the center of the SMF, as seen in the figure. In the second step, an FBG was inscribed in the SMF core covering the hollow cavity, using the fs laser. This divided the FBG into two sections separated by the hollow cavity (FBG1 and FBG2 in Fig. 1(a). A phase shift was introduced by this hollow cavity positioned between the two FBGs. Figure 1(b) shows an enlarged partial view of the inscribed FBG, demonstrating that FBG1 and FBG2 have the same grating pitch (1.070 μm) corresponding to the second

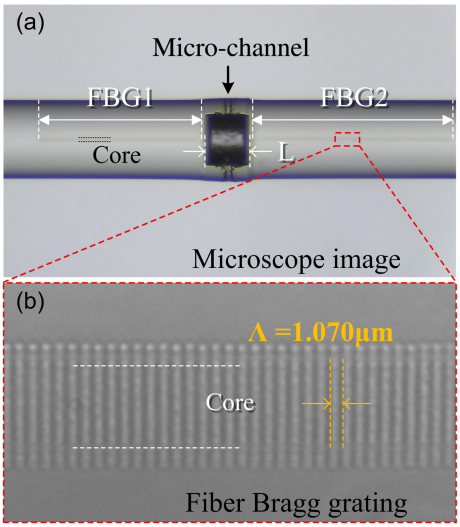

Fig. 1. (a) Optical microscope image of the PS-FBG, modulated by a hollow cavity. (b) Enlarged microscope image of the FBG inscribed using line-by-line etching.

Bragg resonant wavelength at ∼1550 nm. A 40 mW fs laser was focused by a 63× oil objective (NA = 1.4) onto the SMF core during line-by-line FBG inscription. In the third step, a pair of micro-channels crossing the hollow cavity were drilled into the fiber vertically (using the fs laser) to allow gas flow in or out of the device. The diameter of these micro-channels was ∼15 μm.

The spectral properties of this PS-FBG were measured using a 3 dB coupler, a supercontinuum source (SC source, YSL Photonics), and an optical spectrum analyzer (OSA, YOKOGAWA, AQ6317C) with a resolution of 0.02 nm. The presented fabrication process produced a sensor with a grating pitch of 1.070 μm, a grating pitch quantity of 300, and a hollow cavity length of 68.1 μm (using an fs laser power of 40 mW). Figure 2(a) shows the corresponding transmission and reflection spectra over a wavelength range of 1540–1560 nm. It is evident that an approximate π-phase-shift peak with an FWHM of ∼1.6 nm was induced near the center of the FBG stop band at 1550 nm. For comparison, an FBG sample was etched using the same processing parameters (i.e., 1.070 μm grating pitch, 300 grating count, and 40 mW fs laser). The FBG transmission spectrum, which exhibits a central wavelength of 1550 nm and an FWHM of ∼3.3 nm, is shown in Fig. 2(b). This FWHM value is much larger than that of the PS-FBG (∼1.6 nm) shown in Fig. 2(a). It is also clear that the PS-FBG has a higher spectral finesse than the FBG, which can be further enhanced by increasing the reflectivity of FBG1 and FBG2, as shown in Fig. 3(a). A second PS-FBG sample was fabricated with a grating pitch quantity of 1850, a hollow cavity length of 41.9 μm, a bandwidth of ∼212 pm, and a phase-shift peak Q-factor of ∼7302. This device, shown in Fig. 3(a), demonstrates that the finesse of the PS-FBG can be further enhanced by increasing the pitch quantity. The central wavelength λ of the second-order FBG can be acquired using the following formula [19]:

$$m\lambda = 2n_{\text{eff}}\Lambda, \tag{1}$$

where m is the grating order number, n_{eff} is the effective refractive index (RI) of silica, and Λ is the grating pitch. The FBG peak resonance wavelength could be controlled by modifying

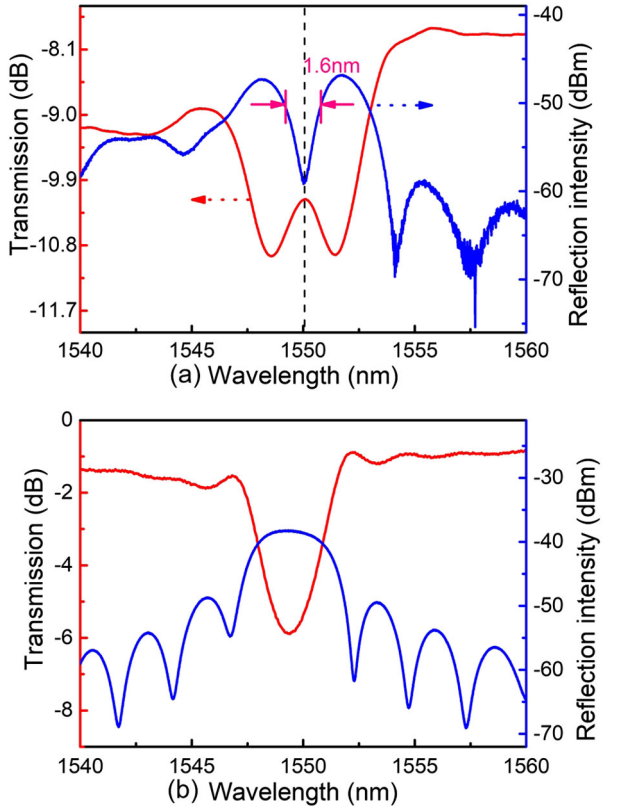

Fig. 2. (a) Transmission (red line) and reflection (blue line) spectra for the PS-FBG fabricated by an fs laser. (b) Transmission (red line) and reflection (blue line) spectra for the FBG.

the grating pitch. As such, a series of PS-FBGs were fabricated with the same parameters (grating pitch quantity, 300; cavity length, ∼70 μm.), with a working wavelength of 1505.7, 1549.7, and 1592.5 nm, corresponding to grating pitches of 1.040, 1.070, and 1.100 μm, respectively [see Fig. 3(b)]. This suggests the sensor grating pitch could be customized to eliminate dependence on the light source wavelength.

Sensor response to variable gas pressure was investigated using a 3 dB coupler, a SC source, an OSA, and a gas pressure controller and meter (PACE6000, Druck). A PS-FBG sensor sample was fabricated with a grating pitch quantity of 300, a hollow cavity length of 68.1 μm, and a pair of micro-channels with diameters of ∼15 μm to allow external gas flow. The sensor was placed in a gas chamber, where the pressure was controlled using a high-precision PACE6000. The chamber was fitted with a feed-through channel, sealed by an adhesive glue, to extend the fiber outside the chamber for real-time measurements.

Figure 4(a) shows the evolution of the PS-FBG reflection spectra as the gas pressure increased from 0 to 2.25 MPa in increments of 0.25 MPa, remaining at each step for 10 min at room temperature. Figure 4(b) shows a linear fit of the experimental data used to calculate the slope (i.e., gas pressure sensitivity), expressed as a ratio of phase-shifted wavelength variations to changes in gas pressure. This value was calculated to be ∼0.77 nm/MPa. As seen in Fig. 4, the phase-shifted dip moved toward longer wavelengths as the gas pressure increased, due to increasing gas RI in the air cavity. The phase-shifted value φ in this experiment was given by [20]

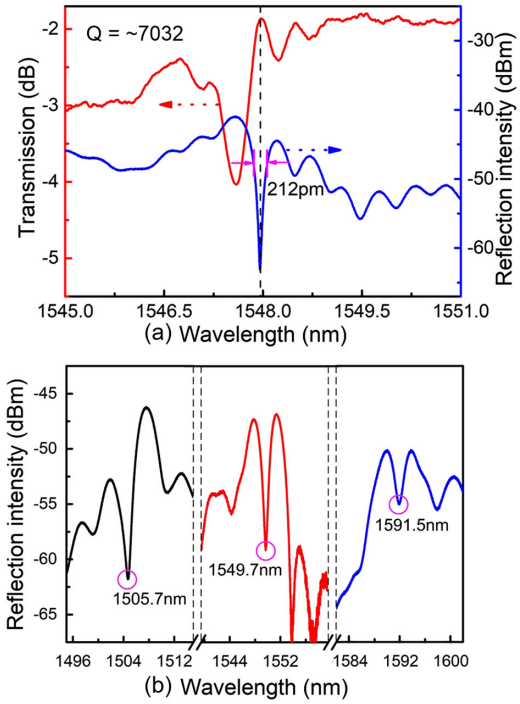

Fig. 3. (a) Spectrum of samples with a Q factor up to ~7302, with a grating pitch quantity of 1850. (b) Spectra of PS-FBGs fabricated with three different grating pitch quantities.

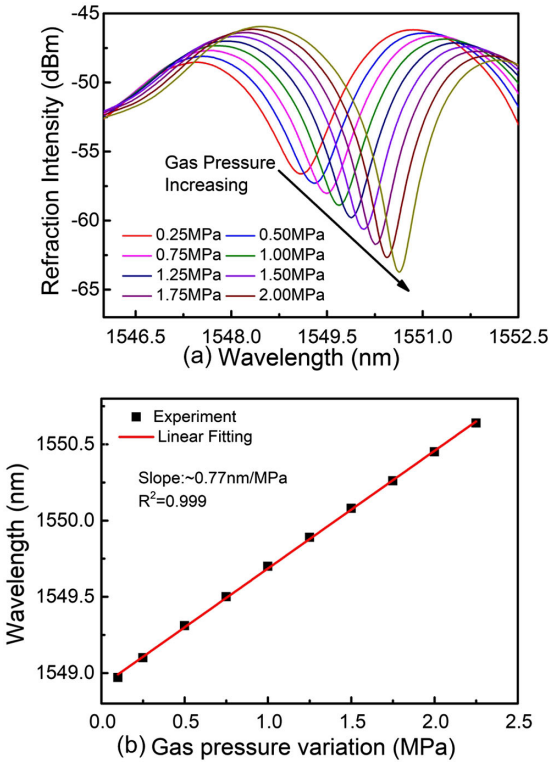

Fig. 4. (a) Reflection spectral evolution of the PS-FBG for different argon pressures. (b) Linear relationship between wavelength variation in the phase-shift peak and gas pressure variation in the cavity, with a slope of ~ 0.77 nm/MPa.

$$\varphi = \frac{2\pi n_{\text{gas}} L_0}{\lambda} + \frac{n_0 \tanh(\pi n_1 L_1/\lambda)}{n_1} + \frac{n_0 \tanh(\pi n_2 L_2/\lambda)}{n_2}, \tag{2}$$

where n_{gas} is the RI of the argon in the hollow cavity, n_1, n_2, and n_0 are the effective RI of FBG1, FBG2, and the fiber core, respectively. In this configuration, a phase shift was introduced by the hollow cavity positioned in the gas RI modulation region between the two FBGs. The degree of this phase shift depends on the gas RI inside the hollow cavity and the lengths of FBG1 (L_1), FBG2 (L_2), and the hollow cavity (L_0). According to Eq. (2), the relationship between the phase shift $\Delta\varphi$ and changes in the gas RI Δngas can be expressed as

$$\Delta\varphi = \frac{2\pi L_0}{\lambda}\Delta n_{\text{gas}}. \tag{3}$$

This equation provides a ratio of phase shift variations to changes in gas RI inside the hollow cavity. It is evident from this expression that phase shifts gradually accumulate as the RI increases, in agreement with experimental results (the peak trending toward longer wavelengths).

The relationship between sensitivity, cavity length, and grating pitch quantity were investigated in an effort to improve the gas pressure response of the proposed PS-FBG sensor. As shown in Fig. 5(a), a series of sensors were fabricated with the same grating pitch quantity (550), but different hollow cavity lengths (33, 70.9, and 95.3 μm). Their corresponding responses were measured, producing sensitivity values of 0.46, 0.64, and 0.85 nm/MPa, respectively. It is evident from these results that gas pressure sensitivity can be enhanced by increasing the hollow cavity length. Similarly, a second series of sensors were produced with a cavity length of ~65 μm, but different grating pitch quantities (450, 550, 650, and 750). Their sensitivities were calculated by linear fitting to be 0.65, 0.64, 0.53, and 0.36, respectively. This indicates that gas pressure sensitivity can be improved by reducing the grating pitch quantity. Based on these data, an improved sample with an increased hollow cavity length (~88.3 μm) and reduced grating pitch quantity (300) achieved a sensitivity of 1.22 nm/Mpa.

The influence of temperature was investigated by placing the sensor in a controllable thermostat and gradually increasing the temperature from 25°C to 95°C, with a step size of 10°C at atmospheric pressure. The corresponding reflection spectral evolution is shown in Fig. 6(a). Three marked points (A, B, and C) on the PS-FBG spectrum were selected to illustrate the temperature response of the sensor. As shown in Fig. 6(b), the measured temperature sensitivity of these three marked points was calculated to be about 9.46, 9.69, and 8.92 pm/°C, respectively. The measured values of points A and B are similar to results reported previously [19], which are mainly affected by the temperature on the FBG, i.e., the photo-thermal effect. However, the temperature sensitivity of point C is a bit lower than the measured values on A and B, and the average difference of them are calculated to be about 0.7 pm/°C. The measured C value represented the PS-FBG peak, and it is contributed to both the FBG's photo-thermal effect and gas RI changes inside the hollow cavity with temperature increasing. Considering the average difference and FBG's working bandwidth, we can predict that the PS-FBG peak would continue to work until the FBG fails, while the fiber suffers the melting temperature.

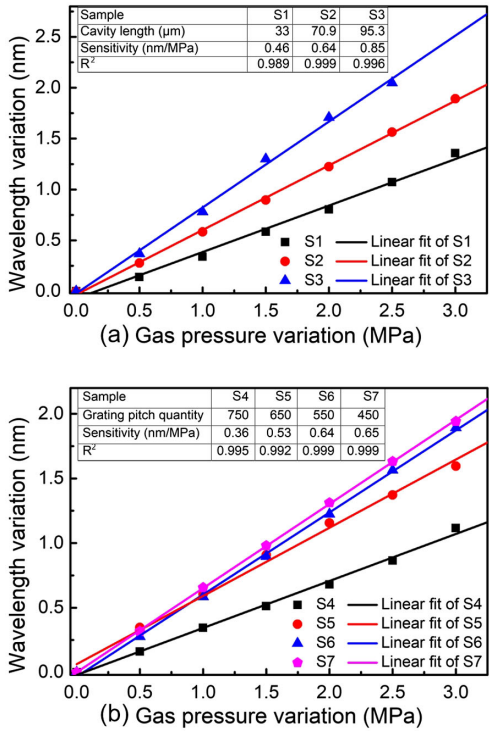

Fig. 5. (a) Three samples with a grating pitch quantity of 550. The gas pressure sensitivity of samples varied with differing cavity lengths. (b) Sensitivity increased with a decreasing grating pitch quantity for a constant cavity length.

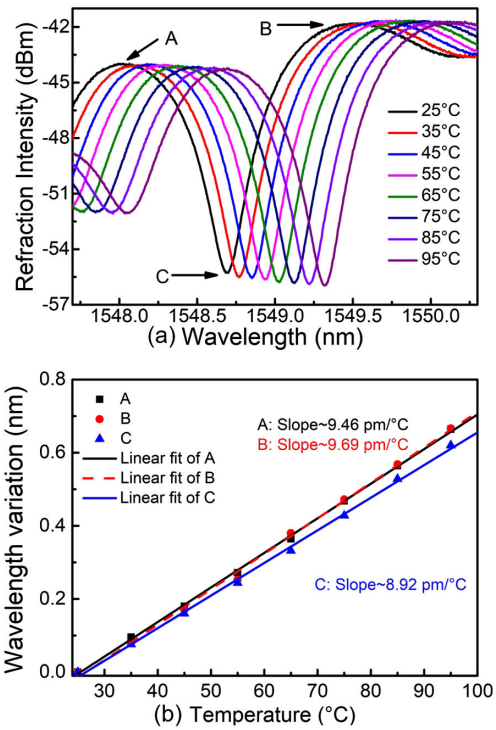

Fig. 6. (a) Reflection spectral evolution of the PS-FBG, subject to different temperatures. (b) Linear relationship between the wavelengths of three peak points in the reflection spectrum and the ambient temperature.

In conclusion, a high-sensitivity PS-FBG gas pressure sensor was proposed and demonstrated in this Letter. The device was modulated by a hollow cavity fused between two SMFs and inscribed using line-by-line femtosecond laser etching. A pair of micro-channels were drilled by the laser to allow gas flow in and out of the hollow cavity. This sensor exhibited a high spectral finesse, e.g., a Q-factor calculated to be ~7302, and the sensitivity was further enhanced from 0.36 to 1.22 nm/Mpa by decreasing the FBG pitch quantity and increasing the hollow cavity length. The proposed PS-FBG sensor also exhibits a low temperature sensitivity of 8.92 pm/°C, which reduces the cross sensitivity between gas pressure and temperature. The sensitivity and spectral finesse of this device could be further enhanced by balancing the hollow cavity length and pitch quantity for applications in dynamic gas pressure sensing.

Funding. National Natural Science Foundation of China (61905165); Education Department of Guangdong Province (2018KQNCX219); Shenzhen Science and Technology Innovation Commission (JCYJ20160427104925452, JCYJ20170818093743767); Development and Reform Commission of Shenzhen Municipality.

Disclosures. The authors declare no conflicts of interest.

REFERENCES

1. D. Tang, D. Yang, Y. Jiang, J. Zhao, H. Wang, and S. Jiang, Opt. Laser. Eng. **48**, 1262 (2010).
2. M. G. Xu, L. Reekie, Y. T. Chow, and J. P. Dakin, Electron. Lett. **29**, 398 (1993).
3. J. Tang, G. Yin, C. Liao, S. Liu, Z. Li, X. Zhong, Q. Wang, J. Zhao, K. Yang, and Y. Wang, IEEE Photon. J. **7**, 1 (2015).
4. B. Xu, Y. M. Liu, D. N. Wang, and J. Q. Li, J. Lightwave Technol. **34**, 4920 (2016).
5. D. Duan, Y. Rao, and T. Zhu, J. Opt. Soc. Am. B **29**, 912 (2012).
6. X. Yang, Q. Zhao, X. Qi, Q. Long, W. Yu, and L. Yuan, Sens. Actuators A Phys. **272**, 23 (2018).
7. J. Ma, J. Ju, L. Jin, and W. Jin, IEEE Photon. Technol. Lett. **23**, 1561 (2011).
8. C. Liao, S. Liu, L. Xu, C. Wang, Y. Wang, Z. Li, Q. Wang, and D. N. Wang, Opt. Lett. **39**, 2827 (2014).
9. J. Ma, W. Jin, H. L. Ho, and J. Y. Dai, IEEE Photon. Technol. Lett. **37**, 2493 (2012).
10. W. Wang, N. Wu, Y. Tian, C. Niezrecki, and X. Wang, Opt. Express **18**, 9006 (2010).
11. S. Liu, Y. Wang, C. Liao, Y. Wang, J. He, C. Fu, K. Yang, Z. Bai, and F. Zhang, Sci. Rep. **7**, 787 (2017).
12. M. Malak, F. Marty, N. Pavy, Y. Peter, A. Liu, and T. Bourouina, J. Microelectromech. Syst. **21**, 171 (2012).
13. M. Jiang, Q. Li, J. Wang, Z. Jin, Q. Sui, Y. Ma, J. Shi, F. Zhang, L. Jia, W. Yao, and W. Dong, Opt. Express **21**, 3083 (2013).
14. M. Li, H. Li, and Y. Painchaud, Opt. Express **16**, 19388 (2008).
15. S. Loranger, A. Tehranchi, H. Winful, and R. Kashyap, Optica **5**, 295 (2018).
16. Y. Shao, X. Han, M. Li, and M. Zhao, Opt. Lett. **43**, 1199 (2018).
17. B. Jiang, H. Dai, Y. Zou, and X. Chen, Opt. Express **26**, 12579 (2018).
18. J. Guo, S. Xue, Q. Zhao, and C. Yang, Opt. Express **22**, 19573 (2014).
19. S. J. Mihailov, C. W. Smelser, D. Grobnic, R. B. Walker, P. Lu, H. Ding, and J. Unruh, J. Lightwave Technol. **22**, 94 (2004).
20. Y. O. Barmenkov, D. Zalvidea, S. Torres-Peiró, J. L. Cruz, and M. V. Andrés, Opt. Express **14**, 6394 (2006).